

MicroFluID - A Multi-Chip RFID Tag for Interaction Sensing Based on Microfluidic Switches

WEI SUN, Institute of Software, Chinese Academy of Sciences, China
 YUWEN CHEN*, Institute of Software, Chinese Academy of Sciences, China
 YANJUN CHEN, Institute of Software, Chinese Academy of Sciences, China
 XIAOPENG ZHANG, Tsinghua University, China
 SIMON ZHAN, University of California, Berkeley, United States
 YIXIN LI, Institute of Software, Chinese Academy of Sciences, China
 JIECHENG WU*, Institute of Software, Chinese Academy of Sciences, China
 TENG HAN[†], Institute of Software, Chinese Academy of Sciences, China
 HAIPENG MI, Tsinghua University, China
 JINGXIAN WANG, Carnegie Mellon University, United States
 FENG TIAN, Institute of Software, Chinese Academy of Sciences, China
 XING-DONG YANG, Simon Fraser University, Canada

RFID has been widely used for activity and gesture recognition in emerging interaction paradigms given its low cost, light-weight, and pervasiveness. However, current learning-based approaches on RFID sensing require significant efforts in data collection, feature extraction, and model training. To save data processing effort, we present MicroFluID, a novel RFID artifact based on a multiple-chip structure and microfluidic switches, which informs the input state by directly reading variable ID information instead of retrieving primitive signals. Fabricated on flexible substrates, four types of microfluidic switch circuits are designed to respond to external physical events, including pressure, bend, temperature, and gravity. By default, chips are disconnected into the circuit owing to the reserved gaps in transmission line. While external input or status change occurs, conductive liquid floating in the microfluidics channels will fill the gap(s), creating a connection to certain chip(s). In prototyping the device, we conducted a series of simulations and experiments to explore the feasibility of the multi-chip tag design, key fabrication parameters, interaction performance, and users' perceptions.

CCS Concepts: • Human-centered computing → Interaction devices.

*Also a member of School of Computer Science and Technology, University of Chinese Academy of Sciences, Beijing, China.

[†]Contact author.

Authors' addresses: Wei Sun, sunwei2017@iscas.ac.cn, Institute of Software, Chinese Academy of Sciences, Beijing, China; Yuwen Chen, Institute of Software, Chinese Academy of Sciences, Beijing, China; Yanjun Chen, Institute of Software, Chinese Academy of Sciences, Beijing, China; Xiaopeng Zhang, Tsinghua University, Beijing, China; Simon Zhan, University of California, Berkeley, Berkeley, California, United States; Yixin Li, Institute of Software, Chinese Academy of Sciences, Beijing, China; Jiecheng Wu, Institute of Software, Chinese Academy of Sciences, Beijing, China; Teng Han, Institute of Software, Chinese Academy of Sciences, Beijing, China, hanteng@iscas.ac.cn; Haipeng Mi, Tsinghua University, Beijing, China; Jingxian Wang, Carnegie Mellon University, Pennsylvania, Pittsburgh, United States; Feng Tian, Institute of Software, Chinese Academy of Sciences, Beijing, China; Xing-Dong Yang, Simon Fraser University, British Columbia, Burnaby, Canada.

Permission to make digital or hard copies of all or part of this work for personal or classroom use is granted without fee provided that copies are not made or distributed for profit or commercial advantage and that copies bear this notice and the full citation on the first page. Copyrights for components of this work owned by others than ACM must be honored. Abstracting with credit is permitted. To copy otherwise, or republish, to post on servers or to redistribute to lists, requires prior specific permission and/or a fee. Request permissions from permissions@acm.org.

© 2022 Association for Computing Machinery.

2474-9567/2022/9-ART141 \$15.00

<https://doi.org/10.1145/3550296>

Additional Key Words and Phrases: RFID sensing, activity and gesture recognition, microfluidic switch circuits, multi-chip RFID

ACM Reference Format:

Wei Sun, Yuwen Chen, Yanjun Chen, Xiaopeng Zhang, Simon Zhan, Yixin Li, Jiecheng Wu, Teng Han, Haipeng Mi, Jingxian Wang, Feng Tian, and Xing-Dong Yang. 2022. MicroFlUID - A Multi-Chip RFID Tag for Interaction Sensing Based on Microfluidic Switches. *Proc. ACM Interact. Mob. Wearable Ubiquitous Technol.* 6, 3, Article 141 (September 2022), 21 pages. <https://doi.org/10.1145/3550296>

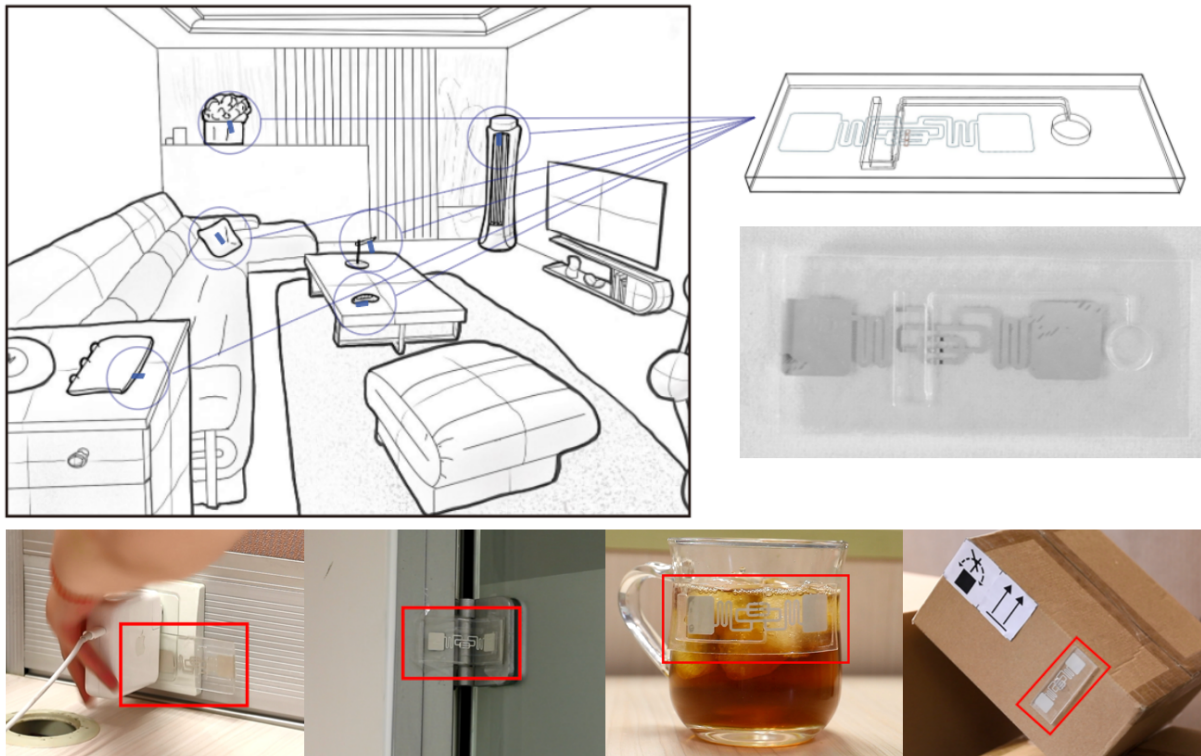


Fig. 1. MicroFlUID is a novel RFID sensing artifact based on microfluidic switch mechanism and multiple IC chips for user activity and gesture recognition. This figure illustrates several scenarios under which our tags could be applied. Starting from the left: the Pressure tag is used to detect whether the plug has come loose; the Bend tag is used to detect the opening and closing state of the door; the Temperature tag is used to indicate the temperature of beverage; the Gravity tag being used as a reminder of box overturned.

1 INTRODUCTION

Due to its low-cost, lightweight, and battery-free characteristics, passive RFID (Radio Frequency Identification) is widely engaged in sensing everyday activity and gestural input wirelessly [? ? ? ?]. Traditional RF based sensing shares a common approach that extracts and analyzes primitive information carried by the wireless signal, e.g., RSSI and phase reported by RFID readers. In such cases, handling signal variances caused by adverse environment and human subject information unrelated to gestures becomes an important yet challenging issue.

As numerous previous work that adopted machine learning methods are normally restricted to heuristic feature extractions [?], recent researches tend to apply deep learning to mitigate the challenges of environment independent and user invariant gesture sensing via modeling variant features [? ? ? ?]. Nonetheless, other concerns may arise from deep learning approaches in practice, e.g., heavy tasks in data collection and high computational costs.

This paper looks into an alternative approach of RFID based sensing that directly informs a user's input state via retrieving multiple ID information instead of primitive signals, which helps to save data collection and training efforts. Driven by this intention, we present MicroFluID, a novel RFID sensing artifact based on configured microfluidic switch mechanism and antenna with multiple IC chips for user activity and gesture recognition. The chips are disconnected from the antenna by default. The antenna structure is modified (i.e., connecting or disconnecting to a chip) by employing the embedded microfluidic mechanism that drives the flow of conductive liquid in response to physical deformation (e.g., pressed, bent), or state change (e.g., weight, angle, temperature). Different from previous attempts that electrically or mechanically switching the presentation of various IDs encoded with measured parameters such as temperature [?], humidity [?], contact and touch event [? ?], MicroFluID contributes the design and fabrication of the microfluidic mechanism to connect and break with multiple chips, which act as part of the switch circuit. The switchable IDs of the tag are mapped to specific input events, and therefore interaction information can be simply retrieved by reading the IDs. The resulting RFID tag is able to reversibly respond to multiple external physical events at a coarse granularity, such as pressing, bending, gravity and temperature.

This work is the first to explore the feasibility of RFID sensing for interaction detection via embedding a microfluidic switch structure. The option of RFID antenna was considered while a typical dipole square-shaped antenna was found suited for its wide use and being easy to be modified structurally to embed multiple chips. The dedicated antenna was screen printed on thin PET film, then bonded seamlessly to a PDMS substrate embedding the microfluidic switch channels. In our design, water was used as the conductive liquid flow inside the micro channels for its non-adhesive feature. Current work finalized a design that works with three chips enabling at most 6 input status, and four types of microfluidic switch channels to detect pressure, bend, gravity and temperature shift, respectively.

During the process of the design, we conducted simulation tests via HFSS to analyze the performance of key design factors including multi-chip pattern of the antenna, conductive liquid, printing material, and microfluidic switch circuits. Afterward, we conducted experiments to assess the feasibility of the four MicroFluID prototypes. Firstly we tested the limited perception distance of the four prototypes, then we calculated the recognition rates in certain measurement periods (0.5s, 0.1s and 0.05s) and valid reads in 1s under a fixed sampling frequency. The results of both tests illustrated that MicroFluID was quite feasible in daily activity and gesture recognition in a regular-sized room. Besides, we repeatedly deformed the artifacts to figure out whether they would fatigue, hence to examine the benefits and drawbacks of our design and fabrication scheme. The experiment procedure and data would be shown in the Feasibility Assessment section. Finally, we carried out a user study that compared MicroFluID with other sensing approaches achieving the same functions, to observe how MicroFluID could benefit novel users, and how users perceive the technique.

This paper presents the following contributions: i) MicroFluID as a novel RFID sensing artifact to retrieve switchable ID information corresponding to external physical events based on microfluidic switch circuits; ii) design and fabrication of the switchable antenna with microfluidic structures to respond to user's input or status change, for example pressing, bending, gravity and temperature changing; iii) tests to assess the feasibility of MicroFluID in aforementioned sensing modalities.

2 RELATED WORK

In this section, we looked into previous work on RFID-based interactions, reconfigurable RFID design, and microfluidics sensing.

2.1 RFID Based Activity and Gesture Sensing

We have seen rich literature on developing RFID-based wireless techniques for user activity recognition and gesture monitoring. Past solutions use machine learning techniques to enable discrete gesture and user activity classification, including speech recognition [?], well-defined hand movements [?], and free-weight exercise [?]. However, machine learning approaches require training overheads and calibrations before the deployment of the systems. While recently proposed RFID systems enable continuous fine-grained tracking without applying machine learning, e.g., body skeleton tracking [?], curvature sensing [?], finger touch tracking [?], these approaches need to create sophisticated mathematical models of the phase and signal strength of the tag signals.

Researchers also looked into novel interaction opportunities enabled by wireless sensing capabilities of RFID, e.g., to support tangible interactions by instrumenting passive tags on objects. Li et al. [?] turned paper into an interface medium with tags that reacted to user manipulations like touch, cover and move. To detect touch, the finger functioned as part of the antenna to turn on the connected chip. This method was also used in establishing a touchpad by Hsieh et al. [?]. Liang et al. [?] used magnet-biased reed switch integrated RFID to sense contact events by detecting appearances of IDs. Similarly, Hsieh et al. [?] leveraged contact switch to sense ID associated event, i.e., stacking a block. By instrumenting the tags on the human body, Liang et al. [?] explored the designs of finger-worn RFID motion tracking for activity recognition on tagged objects. Wang et al. [?] traced the trajectory of an RF source attached to a pen or a finger splint with multiple antennas to enable users to write in the air.

2.2 Reconfigurable RFID

Reconfigurable antennas are of considerable significance in leaning today's wireless technology towards being more compact and low-cost. A reconfigurable antenna is capable of having mechanical, electrical, optical, and material modifications. The modifications change their properties like resonant frequency, radiation pattern, polarization [?]. In the case of RFID, reconfigurability tends to be integrated to sense the motions of the tagged objects as well as of the nearby environment. Works integrating electrical switches to enable RFID-based sensing has become a popular trend in recent years in the RFID industry. For instance, previous work has used temperature-sensitive materials like liquid crystal elastomers, thermal switches, or shape memory polymers for multiple temperature threshold violation monitoring [? ? ? ? ? ?]. The reconfigurability can be realized by the multi-ID approach, which samples the measured values and transmits in real time a combination of different ID codes [? ? ?]. Katsuragawa et al. [?] used an RFID tag design featuring two half-antennas and multiple RFID chips, to detect different pinch points with thumb and index fingers.

Wang et al. [?] proposed a design that utilized the flow of liquid metal to open or close the switch across the RFID antenna upon surpassing a parameter threshold of temperature or tilt. This is similar to our method in that both systems denoted switches in the antenna gaps to activate/deactivate the RFID tag to provide reliable status information. On the other hand, MicroFluID got inspired by Cook's work that proved the compatibility between microfluidics channels and RFID [?], and provided a generic and reversible approach with more levels of sensing granularity to respond to a user's input, which was not achieved before.

2.3 Microfluidic Sensing

Microfluidics is the science of controlling and manipulating fluids precisely on a small scale. For its flexible and stretchable nature, microfluidics is widely applied in the development of biochemical and physiological monitoring sensors on integrated circuits [?????]. Microfluidic systems that assemble sensors and circuits revolutionize electronic system architecture, advanced manufacturing processes, and flexible hybrid semiconductors [?]. By combining soft microfluidic systems with structured adhesive surfaces and controlled mechanical buckling, Xu et al. [?] were able to design stretchable circuit boards with networks of serpentine-shaped interconnects. Leveraging microfluidic chambers and channels, we have also seen a rich set of work that is conducted by stuffing conductive liquids into elastomer microchannels to form sensors [???]. Kubo [?] developed a microfluidic structure made of Polydimethylsiloxane (PDMS) and Ecoflex with different stiffness to improve the stretchability and mechanical stability of RF antennas.

Meanwhile, the potential integration of microfluidics and advanced interface design has been explored by Human-Computer Interaction (HCI) researchers. Lu et al. [?] presented a design space for creating fluidic chambers and channels at millimeter scale for tangible actuated interfaces. Han et al. [?] used tunable flow motion in a fluidic channel to render vibrations like tactile feedback on skin. One notable work closely related to ours is Mor et al. [?], where fluidic channels were utilized to design venous structures that respond to deformation by mechanical inputs from the user. MicroFlUID got inspired by this, and extended it by specifying the fluidic structural design of a switchable portion of the RFID antenna. Recently, Sun et al. [?] leveraged microfluidic channels to reconfigure geometry as well as the functions of an electrode. Tokuda et al. [?] demonstrated interactive and reconfigurable electronic components via a DIY fabrication approach with liquid-metal and other electrolytic fluids.

MicroFlUID exploited the characteristics of microfluidics that the directed transport of minute volumes of liquids can be precisely controlled upon physical deformation (e.g., pressure, bending), or state change (e.g., weight, temperature). Our dedicated design of the switch circuit empowered the RFID tag with various reliable sensing capabilities.

3 MICROFLUID DESIGN

We propose MicroFlUID as a novel RFID sensing artifact that captures ID switches for undergoing reversible press, bend, tilt, or induced temperature change. Such a multi-chip strategy, with an example of an RFID tag consisting of a reconfigurable antenna and multiple chips, requires carefully designed antenna configurations and arrangements of the chips to transmit reliable signals and increase the power transferred.

It is possible to achieve more states by increasing the number of chips on the antenna. However, in practice, there is a trade-off between antenna performance such as valid identification distance and interaction sensing granularity. Including more chips on the antenna would induce less energy distributed on each chip, and more varied resonant frequency of the tag owing to impedance mismatch, resulting in a shorter distance in identification. Thus, to balance the functionality of the sensors and antenna performance, and to save resonant frequency tuning effort which is out of this paper's scope, we decide to settle down to a three-chip structure for initial concept validation and performance evaluation.

3.1 A Three-Chip Antenna Design

The key challenge of antenna design is to receive signals from three chips at the same time and activate them one by one or simultaneously. There are two major approaches to integrating chips with antennas. One is multi-chips in multi-antenna; each antenna can be paralleled next to each other, enabling further modifications (adding or removing chips are easy). However, disadvantages are inevitable when multiple chips are paralleled, meaning chips' activation direction and energy feeding would interfere. The number of chips and distance between each

paralleled chip contribute to this interference. In practice, all these factors will hamper the actual functionalities of the tag. Thus, in our design, we choose another approach including three chips using the same antenna within a single tag. After specifying one antenna in our structure, we have two potential options for connecting three chips: multi-loop dipole antenna, or multi-loop coupled antenna [?]. Considering that we intend to use microfluidics to control the switching of three chips, the closer the distance between adjacent chips, the more precise the control using microfluidics. We choose to use a multi-loop dipole antenna for easier and better-suited integration of microfluidic switch structures.

Our design is based on a typical dipole square-shaped antenna, which is common in commercial use, easy to modify the structure, and convenient for debugging with an off-the-shelf reader. It runs the standard commercial RFID protocol and operates at an ultra-high frequency (UHF). The square lamina in the antenna design has 17mm in width and 15mm in length. To reduce potential interference that a three-chip structure might cause, especially regarding the impedance mismatch, we kept most of the antenna unchanged and just added two small branches on the chip circuit to connect three chips (Figure 2). Each branch is 10mm long, containing a chip and a gap. The gap is reserved on the antenna next to each chip, which is of 0.5mm, a relatively short length that was chosen after weighing the subsequent production processes while preserving the most original antenna pattern. In such a gap design, chips were disconnected by default and connected when conductive liquid flow into gaps (therefore fill the gaps). Design details of the antenna can be found in Figure 2.

The amount of injected conductive liquid in the channel was carefully controlled. By manipulating injected liquid length to fill up 0.5mm gaps, we enable chips to function in 6 states: the first one, the second one, the third one, the first and the second chip, the second and the third chip, and all chips, labelled red in Figure 2. When two or more chips are connected, the reader receives multiple ID information simultaneously. It is worth mentioning that a single section of liquid can only control a maximum of 5 states (apart from the last state listed above, which requires a longer column of liquid).

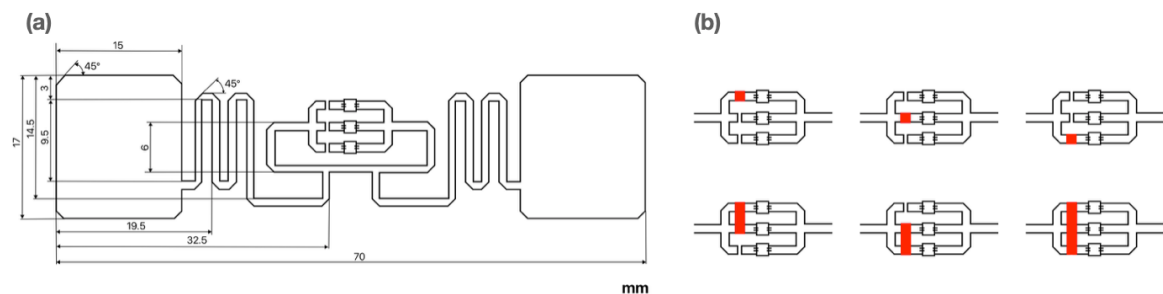


Fig. 2. (a) Antenna design and 6 input states with 3 chips; (b) The gaps filled with liquid droplets are labelled in red which means their connected chips are activated.

To verify the feasibility of the antenna design, we used HFSS to computational simulate its performance. The design of the tag in the simulation is shown in Figure 3(a), where the plates are the main radiators. The meandering line is used to reduce the size of the tag. The metal lines around the ports form a loop that can adjust the impedance matching.

The simulated vector current distribution of the tag at 915 MHz is shown in Figure 3(b), which is very similar to that of a typical dipole. The reason that we chose the bending dipole design over other designs is that under the same resonant frequency it can be shorter and smaller in size which largely reduces the space of the MicroFluID.

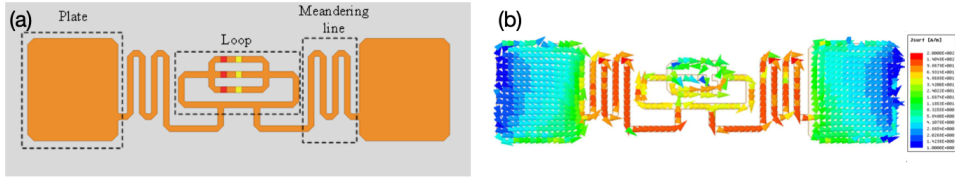


Fig. 3. (a) The configuration of the proposed multi-chip tag; (b)The vector current distribution at 915 MHz.

Though under the same length, our antenna would have a lower radiation frequency compared to the straight-line dipole design. Besides, due to the more complex structure, the impedance of each port and some properties of radiation are unpredictable, making the antenna and chips matching process difficult. Thus, we conducted simulations on our antenna's impedance, E-plane, and H-plane.

Figure 4 represents the input impedance of the proposed tag with different number of chips activated. Considering the impedance of the chip which we used in the MicroFluID is $12.5-j277$ at 915MHz, from the simulation results Figure 4(a, b) we can find that the matching of the antenna will be best when two chips are excited(impedance around 280, resister around 20). The active reflection coefficient curves in Figure 4(c) confirm the judgment. The active reflection coefficients in different states at 915MHz are -8.86 dB, -31.24 dB and -14.66 dB, respectively.

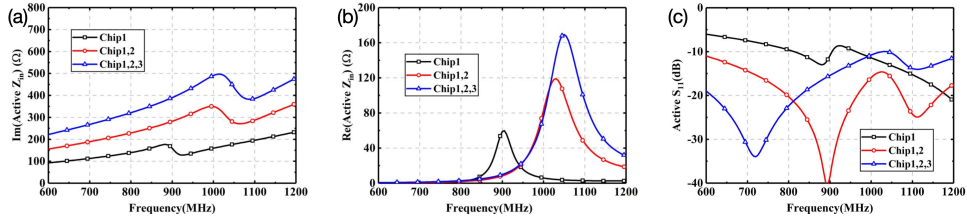


Fig. 4. The simulated input impedance in different states. (a) Impedance; (b) Resistance; (c)The simulated active reflection coefficient in different states.

The radiation patterns of the proposed tag in E-plane and H-plane at 915MHz are shown in Figure 5. The donut-shaped pattern is kept when the antenna works in different states. Because of the difference in matching, the realized gain of the proposed antenna in different connecting conditions are slightly different. The peak gains in different conditions are 1.40 dBi, 1.96 dBi and 1.80 dBi, respectively.

The results of computational simulations demonstrate that the proposed 3-chip design is fairly acceptable for actual using purpose, since in each of 1-chip, 2-chip and 3-chip connected scenarios, the maximum gain appears in the Frequency range of 600 – 1200MHz, which means that the impedance matching requirement is satisfied. The simulation results will be further validated based on the actual performance measurement in a later section.

3.2 Conductive Liquid

We conducted trials to figure out a better choice of conductive liquid among water, and liquid metal. Liquid metal has lower resistance and better electrical properties ($8\Omega/\text{sq}$ for AgNWS (ISP-125); 3.4610^6S/m for Galinstan at 20°C , which contains 68.5% of Ga, 21.5% of In, 10% of Sn. While for water, it is 0.05S/m). However, it easily forms an oxidized layer when exposed to air that sticks to the flow channel (made of PDMS) of that small size (with a width of 1mm). Alternatively, according to Cook's work [?], water is an optional choice for its relatively

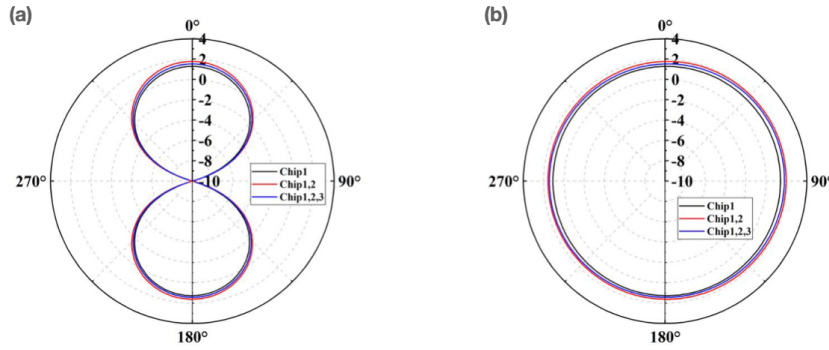


Fig. 5. The simulated radiation patterns at 915 MHz on (a) E-plane and (b) H-plane.

high permittivity (78.4 at 798K), non-adhesive feature, as well as its availability and low cost. A drawback exists as water has relatively poorer conductivity compared to liquid metal, thus inducing higher impedance in the antenna circuit. However, such an effect is limited as the gap is very small. When water was applied, the perception distance was measured 3.6m, 3.5m, and 3.4m when 1, 2, and 3 chips connected, respectively, while the values were 12.1m, 9.8m, and 10.6m respectively when using liquid metal. Tough liquid metal seemed to be the better choice considering the perception distance, we found it clearly influenced the prototype's ability to resume disconnect status due to the viscosity issue. Thus we tried water to find out if it would be acceptable via actual measurement. In the simulation, the material of the printed antenna was Ag with a thickness of about $10\mu\text{m}$, corresponding to the technique (silk-printing, using conductive silver paste) adopted in the later fabrication process.

The result of the measurement is shown in Section 5, as a part of the Hardware Setup.

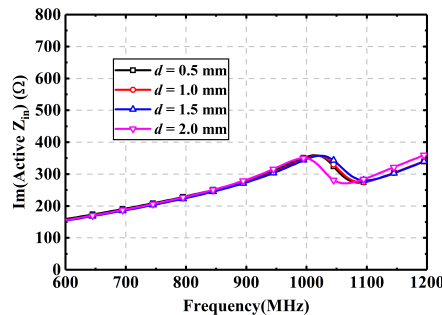


Fig. 6. Impedance value of substrates of 0.5mm, 1mm, 1.5mm and 2mm, under frequency range from 600MHz to 1200MHz.

3.3 Substrate Thickness

Considering the flexibility demand of the whole device and the connective strength between the printed antenna and the substrate, PET membrane (with a thickness of 0.05mm) has been chosen, on which the three-chip antenna will be printed. Another key component of the tag is the microfluidic switch circuit (described in Section 3.4), which is fabricated using PDMS.

3.4 Microfluidic Switch Circuit

MicroflUID includes microfluidic mechanism to build switch circuits, i.e., moving the conductive fluid to connect and disconnect the antenna with the chips. Previous work [?] demonstrated design concept for microfluidic mechanisms to generate visual effects in response to tangible and deformative input. Built upon this, we extended on design and fabrication of the primitive structures of the switch circuit. Other key parameters, such as sizes and materials, also affect the functions proposed to achieve.

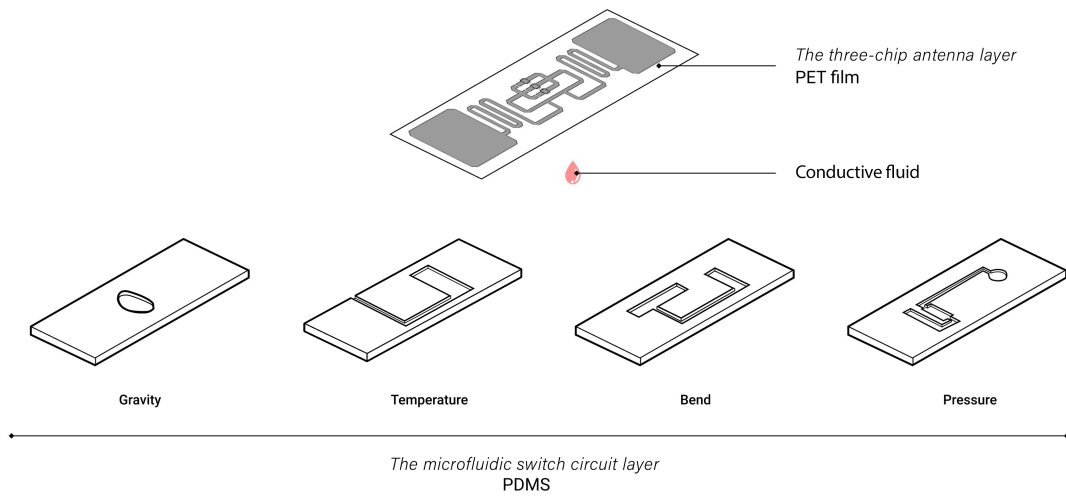


Fig. 7. Concept design of the three-chip antenna, conductive fluid and the microfluidic switch circuit for four types of tags, corresponding to detecting four types of external stimuli.

Considering the high requirement of the flexibility of the prototype, we chose PDMS for the microfluidic channel and PET for the substrate. Based on the same consideration, the thickness of MicroflUID is designed to be as thin as possible. The tag size should be neither too large nor too small, for easily sticking on everyday little things while providing enough room for chips and microfluidic channels. As for the structure, the concept design of four microfluidic switch circuits for their corresponding tags is elaborated as the following and visually presented in Figure 7.

The structure of a microfluidic switch circuit consists of a fluid-moving channel and air chambers. At one or both ends of a fluid-moving channel is connected with air chamber(s), a flat chamber supported by a soft PDMS material and a PET top membrane. As its top membranes are triggered by external inputs to contract significantly, the volume of the air enclosed decreased. The tags obtained two chambers. One is the acceptor chamber, to detect external deformation. The other is the receptor chamber, to be tuned in regards to achieving designed unbalanced forces. A gravity tag had only one chamber, which is also its fluid-moving channel.

Fluid-moving channels are designed in millimeters, which is a typical scale of microfluidic systems. Fluid flow in a microfluidic channel is laminar (with a low Reynolds number < 1100), where viscous forces dominate inertia forces. To allow liquid droplets to flow in the enclosed channel, we consider Pascal's Law [?], to instrumentally generate a pair of unbalanced acting forces on two sides of the liquid. When external environmental detection

occurs, an unbalanced acting force is present and drives the inserted liquid to move at a certain displacement. To drive the liquid moving exactly to chips' activation ports, the width of the fluid-moving channel should be greater than the width of antenna gaps in order to allow droplets to pass through antenna gaps and make sufficient contact with both sides of antenna gaps to connect the circuit.

We set the position of chips' activation ports and initial position of injected fluid accordingly to ensure the circuit working. In the construction of tags, the final position of the inserted liquid has to surpass the position of the furthest-chip activation port. The maximized final position is controlled using the following working principle: generally the larger the surface area of acceptor chambers, the larger the forces differences generated, resulting in more significant displacement.

Several parameters are set to help understanding: d , displacement of the inserted liquid; p_i as the initial position of inserted liquid in the channel; p_f as the final position of inserted liquid.

3.4.1 Pressure. In the Pressure-directed (Figure 8) microfluidics channels, when the external force squeezes the thin film on the acceptor chamber causing deformation, the volume inside the acceptor chamber will decrease. Meanwhile, liquid drops move in the opposite direction of where deformation happened and stop when pressure from the acceptor and receptor chamber is balanced. Using the movement of the liquid drop to quantify squeezing intensity, we set three RFID chip activation ports along the path of liquid drop movement. When liquid drop moves through the port, the chip is connected to the antenna and therefore activated. By altering the surface area and depth of the acceptor chamber, we can adjust the sensitivity of pressure detection.

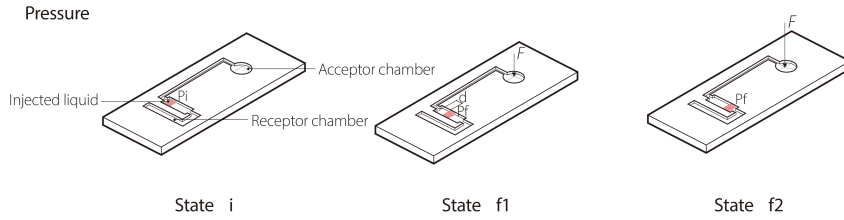


Fig. 8. State changes within the microfluidic switch circuit of a pressure tag, as its acceptor chamber receives external pressure, from an initial state (state i), to the first final state (state f1) when a pressing force is present and the second final state (state f2) when the pressing force increased.

3.4.2 Bend. In the Bending (Figure 9) sensing microfluidics tag, acceptor chamber gets squeezed when the tag is bent, altering the gas pressure within. The structure design for the bending sensor is similar to the design of the pressure sensor. Pressure is balanced initially between two chambers and liquid drops. When bending happened, the acceptor chamber would be squeezed, causing pressure imbalance, pushing the liquid drop forward. Both the PET and PDMS substrates are sufficiently flexible so the tag could be bent in both directions without damage.

3.4.3 Temperature. In Temperature (Figure 10) sensing microfluidics channel, because of the excellent heat conductivity of PDMS substrate, the air inside the channel will expand or contract rapidly corresponding to environmental temperature change. This expansion and contraction will drive the liquid drops to move close to or away from acceptor area. We apply this observation in our Temperature sensing design. The PDMS has favorable heat conductivity, and the mixer of air and liquid can rapidly expand or contract as temperature changes. Thus, we design an air chamber for air contraction and expansion. Besides, we also design multiple RFID chip activation ports along the path of liquid drop movement corresponding to current temperature changes. Applications of temperature sensing tags are broad including simple temperature detection and cold-chain delivery.

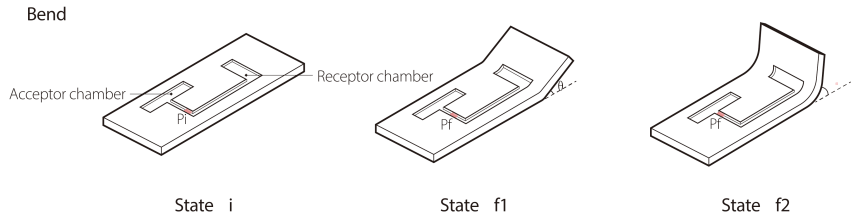


Fig. 9. State changes within microfluidic switch circuit of a bend tag, as its acceptor chamber receives deformation, from an initial state (state i), to the first final state (state f1) when a bending is present and second final state (state f2) when the bending angle increased.

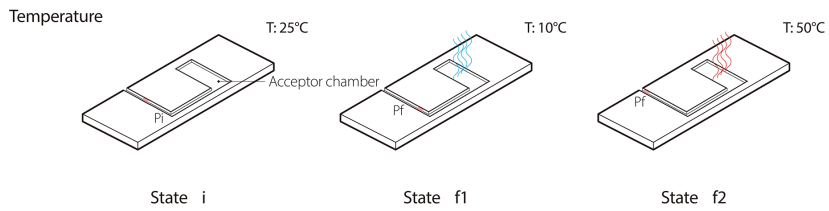


Fig. 10. State changes within microfluidic switch circuit of a temperature tag, as its acceptor chamber perceives temperature changes, from initial state (state i) at room temperature, to first final state (state f1) at a lower temperature (10°C) and second final state (state f2) at a higher temperature (50°C).

3.4.4 Gravity. In the Gravity (Figure 11) sensing microfluidics channel, liquid drops can move freely in part of the channel. When in static mode, the top surface of the liquid inside is horizontal. We also prepare three RFID chip activation ports along the path of liquid drop movement. Liquid can be used to detect the direction of tilting with respect to gravity as they tend to level out horizontally [?]. We leveraged this phenomenon by designing a miniature liquid reservoir with the shape of an irregular rectangle. When the sensor gets tilted, the bubble floats accordingly and connects to the outreach pins causing connection to different chips.

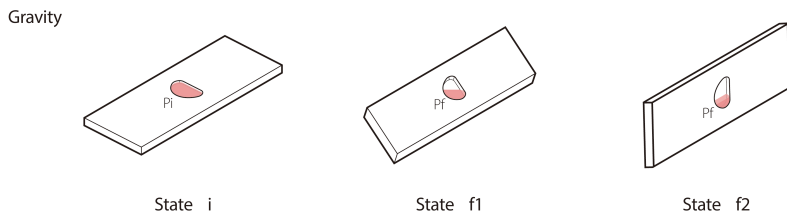


Fig. 11. State changes within microfluidic switch circuit of a gravity tag, as it changes orientation, from initial state (state i) upright orientation to first final state (state f1) at a 45deg orientation and second final state (state f2) at a 90deg orientation.

4 MICROFLUID PROTOTYPE

The prototype of MicroFlUID maintains a two-layer structure. The base layer is made of PET (with a thickness of 0.05mm , above which an RFID antenna is printed and three RFID chips are sticked. The top layer(microfluidic switch circuit) is made of PDMS, consisting of an acceptor chamber, a liquid-moving channel, and a receptor

chamber ($2mm$ in thickness for the pressure, bend and temperature tag, while $2.5mm$ for the gravity tag). The whole tag is $4cm$ in width, $9cm$ in length and about $2mm$ to $2.5mm$ in thickness.

The tag could respond to physical deformations caused by the user's actions, as well as environmental changes such as temperature and orientation. The three chips structure is able to support at most 6 different states identification, which is sufficient to prove the tags' primitive potential and sustains acceptable identification distance. Here, 4 prototypes were designed and fabricated, all of which worked with an off-the-shelf reader. Next, we would elaborate on the fabrication process and the prototypes.

4.1 Fabrication

Considering the properties of PET, silk-screen printing technique was chosen to print the antenna layer and the microfluidic switch circuit layer was fabricated by casting mold technique. The fabrication process is shown in Figure 12.

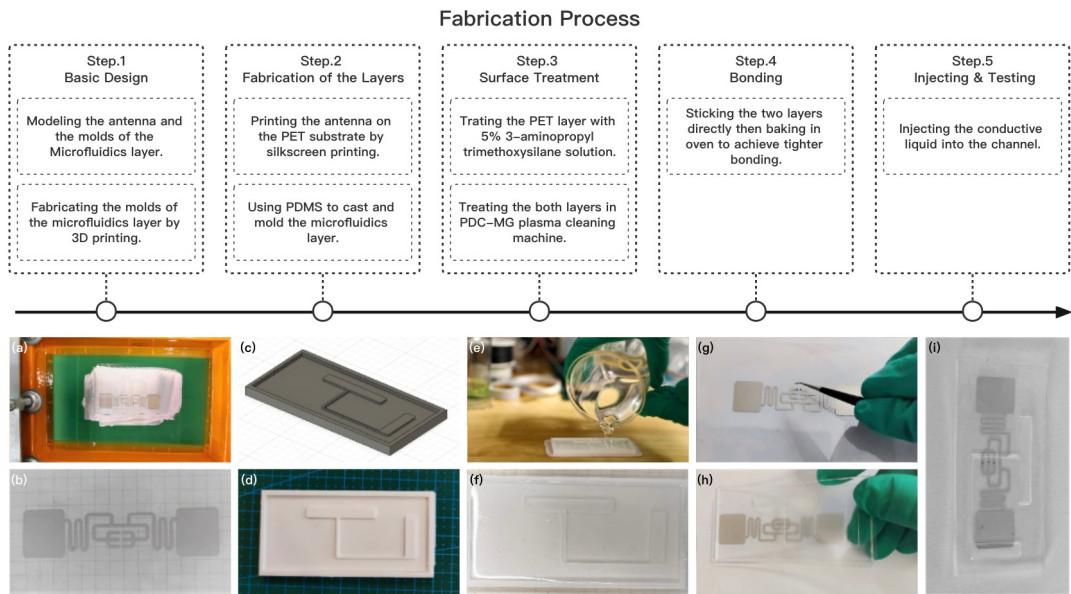


Fig. 12. General fabrication process of the tags. (a) Silkscreen printing process; (b) Silk-printed PET-based antenna layer; (c) Mold model designed by Autodesk Fusion 360 (taking the Bend sensing tag as an example, the same below); (d) 3D printed mold; (e) Pouring liquid PDMS into mold; (f) The cured PDMS layer in its mold; (g) Sticking chips to antenna layer; (h) Bonding two layers together; (i) A whole fabricated sensing tag.

Firstly we used Fusion 360 by Autodesk to computationally model the antenna. Based on our antenna model, we customized a silk-screen with a size of $19cm \times 12cm$, 300 mesh value, $34\mu m$ diameter silk, and $68\mu m$ thickness for printing. The antenna was silk-screen printed on the PET thin layer with $0.05mm$ thickness, which had relative permittivity $\epsilon_r = 2.98 - 3.16$ across the range $0.0006 - 1.0000MHz$. The printing ink we used was nano-silver liquid (ISP-1015) with sheet resistance less than $6m\Omega$ and solids content $70wt\%$. After the antenna had

cured on the substrate, we glued three RFID chips onto the antenna with the same silver liquid mentioned. Besides, we drilled six through-holes and poured the silver liquid into it, so the circuit could be conducted when the conductive fluid flowed in the microfluidic channel on the backside of the film. Then the antenna was baked in the oven under 70°C for 15 minutes.

PDMS (Dow and Corning's Sylgard 184) with agent A cross-linker/curing agent B = 10:1 was used to cast and mold the microfluidics layer. The ratio was determined empirically to maintain a balanced rigidity and flexibility of the final produced PDMS layer. The PDMS was stirred in a flask for over 5 minutes until it became visually milky with tiny air bubbles to ensure thorough mixing. The prepared PDMS was firstly vacuumed in a vacuum desiccator for 20 minutes to remove most of the air bubbles, then cast into a prepared mold and vacuumed again for 10 minutes for the same purpose. The clean and transparent PDMS was cured in an oven (75°C for 2 hours), forming a thin layer of film that can be easily peeled off from the mold.

Next, we bond the two layers tightly to prevent leakage of the conductive fluid and the air in the microfluidic channel. In this step, a PDC-MG plasma cleaning machine and 5% 3-aminopropyl trimethoxysilane solution were used for material surface treatment. The antenna layer had two sides, one was silk-screen printed, and the other was blank. To achieve more compact bond, we chose the blank side, which was processed firstly in a plasma cleaning machine for 2 minutes and then soaked in 50° thermostatic magnetic stirring water bath with 3-aminopropyl trimethoxysilane solution for 30 minutes. After, we processed another 2-minute plasma cleaning. For the microfluidics layer, the same plasma cleaning process was required. We could bond two layers together afterward, and then bake it in the oven under 75°C for at least 1 hour.

The final step was injecting the conductive fluid into the channel by using a medical injection syringe. Notice that the syringe needle should be extremely thin and spiky, so it would not hamper the leak-proofed channel. Then uncured PDMS could be smeared on the pinhole, and a baking process was also applied to further ensure a tight seal. As the precision of 3D printing was only 0.1mm , this would result in a rugged surface on the molds so printed on a microfluidics layer, obstructing the bonding process. To fix this, we smeared a pretty thin layer of PDMS on cured microfluidics layer and then applied baking process to obtain a smoother surface.

4.2 Prototype of the Tags

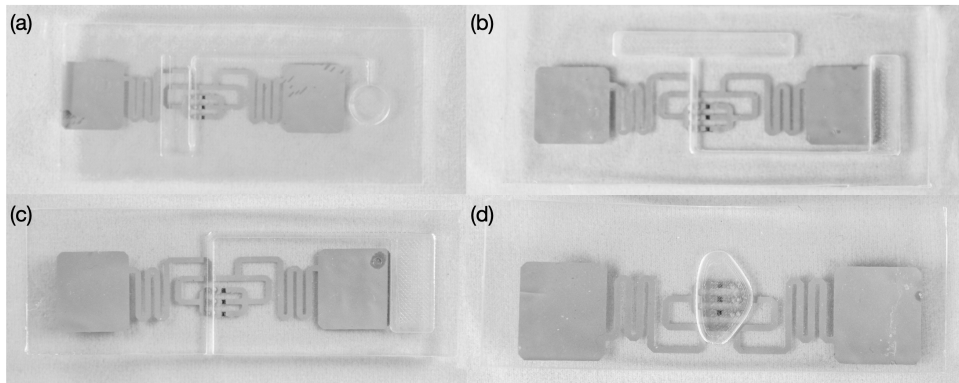


Fig. 13. Prototypes of MicroFluID tags: (a) Pressure tag; (b) Bend tag; (c) Temperature tag; (d) Gravity tag. The fluidics channels were designed 1mm in diameter. However, considering the fabrication deviation, they might be slightly narrower in reality. For the gravity tag, its chamber was about 10mm in width and 20mm in length, representing as an irregular streamline rectangle.

As stated, the flow of our inserted conductive liquid is primary condition of a working circuit. Six corresponding working circuits due to 6 different combinations of the three chips provide six differential statuses for identification. Therefore, mapping the external testing statuses with combinations of three chips is essential to our design. In the following, we present our four types of tag prototypes with different designs of chambers and channels, and use the physical properties of the designs to map with differential statuses.

Figure 13 showed the resulted Pressure tag, Bend tag, Gravity tag, and Temperature tag. On average, each tag measured about 90mm, 40mm, and 2.1mm in length, width, and height respectively (the gravity tag was about 0.5mm thicker), and they weighed around 9.5g. The channels were 1mm in radius for the pressure, bend, and temperature tags. For the gravity tag, the size of its streamline channel was experimentally decided (about 10mm in width and 20mm in length), to guarantee the conducting liquid could flow fluently and respond promptly in the channel when its orientation changes. The antenna impedance difference caused by the microfluidics circuit switch can be ignored since the cavities were designed away from the antenna.

5 FEASIBILITY ASSESSMENT AND USER EVALUATION

As simulations in Section 3 preliminarily indicate the feasibility of design, two quantitative experiments were conducted to further demonstrate the prototypes could also perform well in actual situations, regarding both the reflected signal and the fluid floating within the channel. Besides, we conducted a user study to compare our tags with traditional methods achieving similar functions. In the actual prototypes, parameters such as thickness of PDMS, thickness of silver circuit printed by silk-printing, conductivity of connective port of antenna and chips are unable to be exactly the same as in computational simulations, and actual tests involve way more complexities in environment and EM interferences. Therefore, we took a practical approach and tested the input impedance from middle branch (where chip2 would be loaded) while the gap was filled by water, under frequency ranging from 500MHz to 2000MHz. Then we tested the maximum perceptible distance and accuracy rate in unit time and then analyzed feasibility of our MicroFluID tags only on the basis of our fabricated results, as well as the testing of the ranges and resolution of the four types of tags.

5.1 Hardware Setup

As mentioned in Section 3.2, an actual measurement of fabricated antenna was conducted to test the real and imaginary part of input impedance from middle branch, which corresponds to 1-chip connected scenario(Figure 14). According to the measurement, the imaginary part of water filled antenna was 303.853Ω at the frequency of 912.5MHz, which illustrated that using water to fill the gap could almost achieve impedance matching successfully, compared to the imaginary part value of 277Ω for condition while 2 chips are being activated. Such a result indicated that the antenna was acceptably matched with chips, which guaranteed the tag could generate a fairly strong reflected signal while chips connected were being activated.

To set up a MicroFluID hardware system, we selected an Impinj RFID reader to detect activation states of three chips possessed by each MicroFluID tag. MicroFluID tags are numerously used in an environment in our envisioned applications. An Impinj RFID reader¹ is capable of identifying up to 1254 tags with emitted signal strength greater than $-76.5dBm$ at its static reader mode. It is also capable of electronically connecting to 4 non-reconfigurable antennas simultaneously to expand detection ranges in practical uses. Therefore, the Impinj RFID reader is practically aligned to MicroFluID tags in applications. Besides its advantages of perfect alignment with MicroFluID tags, it also provides wireless channel information assisted with computational packages for secondary development [?].

On computational software ends, MicroFluID's algorithms were implemented in C language and featured with its simultaneous data processing of signals transmitted from hardware ends. For example, when a MicroFluID

¹<https://support.impinj.com/hc/en-us/articles/1500003045181-Impinj-R700-Reader-Modes>

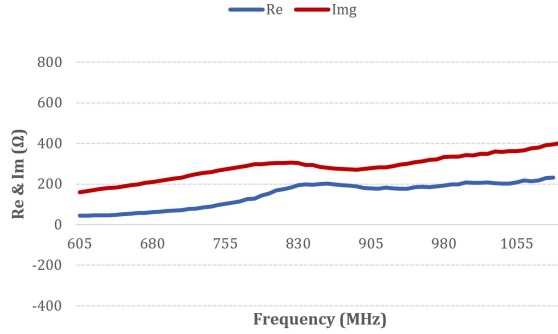


Fig. 14. Input impedance of the antenna, from the middle (where chip 2 is supposed to be loaded) branch.

tag was placed on an object and started to detect events undergone by the object, MicroFluID's algorithms simultaneously updated the data representing correlations between chip ID and events detected.

The experiments were all completed within an empty rectangular-shaped room of 35m^2 . In preparation, an Impinj R700 RAIN RFID reader was connected to a S9028PCL 12dBIC antenna to receive signals from the tag.

5.2 Experiment 1: Evaluation of the Reflected Signals

5.2.1 Process. MicroFluID prototypes were evaluated with a series of tests to observe accuracy and reliability of reflected signals within the tested limited perceptible distances. Figure 15 illustrates the experiment process. Person A holding a tag firstly stood at a rather close distance (0.5m) from the reader and made sure the tag he held was in a fixed mode (certain chip(s) connected by conducting liquid). After confirming the reader could receive the right signal, Person B started to record the data for 60s. Then A changed his position, moving further (1m each time), while B took down the data if the reader could receive valid signals (at least one time of triggering signal per second). If not, A should move back (0.1m each time) until valid read appeared. The farthest position was recorded as perceptible distance. The test was repeated under different states.

The whole experiment about reflected signals was composed of four aforementioned tests for the four types of tags. To make the assessment more concise, we set the tag facing the center of the antenna.

As for fatigue testing, we manually changed each tag's states (6 states for pressing, bending, and temperature tags, 3 states for the gravity tag) 100 times to observe if the structure remained functional after repeated deformation.

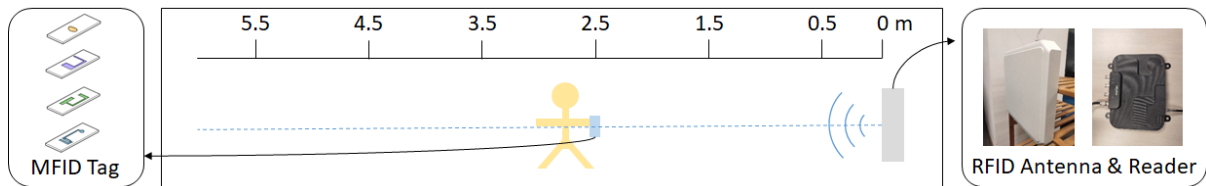


Fig. 15. A sketch map for the experiment setup.

5.2.2 Data Processing. While processing the experimental data, a sliding window algorithm was applied, where windows and steps were assigned the same length. To evaluate data accuracy, we adopted sliding windows/steps

of 0.5s, 0.1s and 0.05s respectively. If a valid signal was recorded within a chosen time period, we assigned YES as the signal was considered to be received while assigning NO otherwise. Accuracy rate was calculated by the proportion of a number of YES windows. On the other hand, to evaluate reliability, we adopted a sliding window of 1s and simply counted the number of times the signal was received in each window, and took average of them. The more times the signal was received (which indicates reflected signals were much substantial), the more reliable the tag tested was.

5.2.3 Experimental Results. The perceptible identification distances were explored (as shown in Figure 16). For all tags, the furthest distances were observed when all chips were activated, and the identification distance dropped sharply as the number of chips conducted decreased, according to which we recommend users to select multiple-chip activated states as priority while using. This result was contrary to general understanding: chips working simultaneously together consume more power than any of them alone. Larger power consumption results in shorter perception distance. However, the impedance matching might cause this problem. Compared with impedance of one chip or two chips in parallel circuits, impedance of three chips in parallel circuits better matched the impedance of the antenna. Such result could be regarded as a partial proof of our simulation results in Section 3.1, where 1-chip loaded circuit appeared to perform the worst.

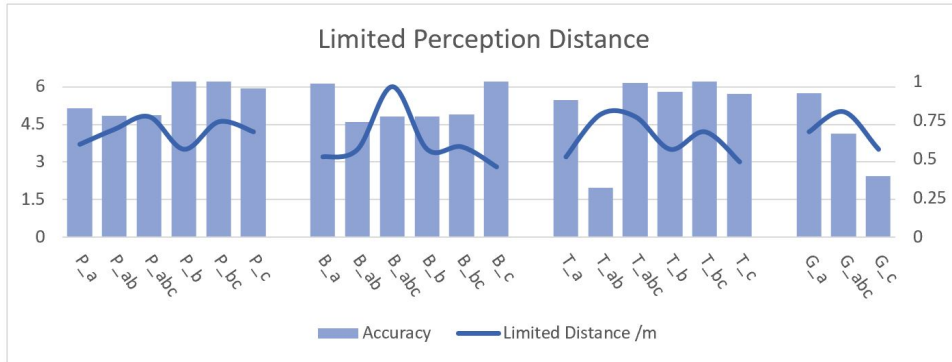


Fig. 16. The perceptible distances of MicroFluID tags under different modes. Window size here was 0.5s. X-axis represented the activating chips of four tags (e.g. 'P_a' means the chip labeled 'a' in the Bend tag was activated. 'P' for 'Pressure', 'B' for 'Bend', 'T' for 'Temperature' and 'G' for Gravity) and y-axis represented distance. Same for Figure 17.

To further evaluate reliability, we calculated the times signals could be read per second for MicroFluID tags while different chips were activated, as shown in Figure 17. The line chart indicated that the farther the testing distance was, the fewer the valid reads were. Besides, among all modes, all activated modes where chip a, b and c were all activated performed the best lative importance.

The limited perception distance of each tag under every state was beyond 2.5m, indicating that they could be used to detect daily activities and gestures with relatively low frequency (below 10HZ) in a 5m × 5m room (if RFID readers are installed on each wall).

5.3 Experiment 2: Limit Test on Range and Corresponding Resolution

This experiment evaluated each tag's interaction capabilities regarding their sensing modalities.

The experiment showed that as the external stimuli adapted larger strength, the liquid underwent bigger displacement. In that, the maximum displacement of the liquid in the channel and the maximized chamber deformation together impact on detection range of our tags. As we only intended to realize a coarse-grained

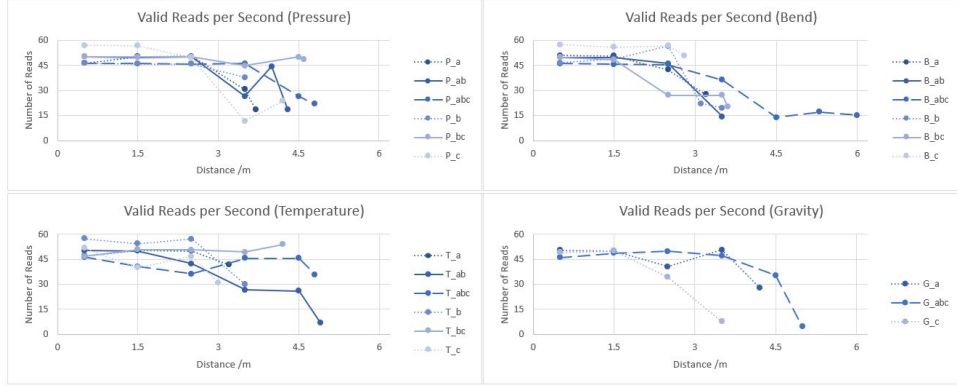


Fig. 17. Valid reads per second, for six modes of each tag (three modes to the gravity tag), under various distances.

sensing device, the resolution would not be that high. Here we define resolution as the change of the value of external stimuli every 2mm the liquid inside moves, which is just the space between each two adjacent chips. We set up sensors to detect both external stimuli and displacements of water inside, described in later paragraphs. The range and the resolution were then inferred from stimuli values and displacements based on linear fitting method.

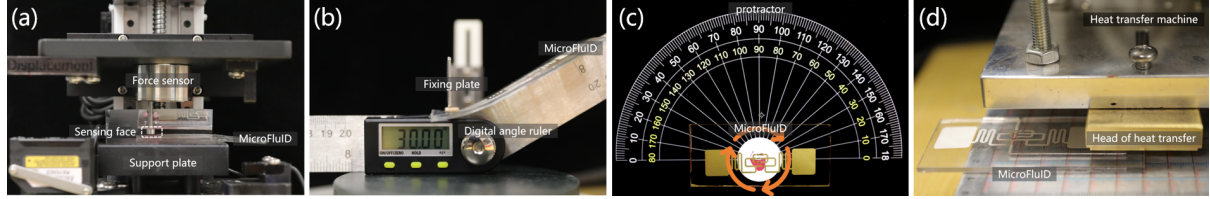


Fig. 18. Evaluation setup of (a) Pressure; (b) Bending; (c) Gravity; and (d) Temperature tags.

5.3.1 Pressure tests. On a vertically motorized pressure-measurement platform, a cylindrical HZC-T force sensor (0-10N) with 8 mm diameter and 10mm height pressed on the tag and a camera recorded the current pressing force and the resultant liquid displacement. Initial position of liquid was recorded in Figure 18. After 10 testings, liquid displaced 2mm corresponding to a 0.02N pressing force, and it reached its maximum as the pressing force was greater than 0.49N. Resolution of the pressing tag was 34 mN.

5.3.2 Bending tests. We fold along a central line of the chamber on a bend tag and recorded bend angles and consequent liquid displacement with a camera. Figure 18(b) reports the initial position of the liquid. Averaging collected data from 10 testing trials, we discovered that the tag bent at 17° as the liquid displaced at 2mm, and 31° was the maximum for the tag to receive signals from the liquid. Tested resolution of the bend tag was 1.2° per millimeter.

5.3.3 Temperature tests. A WT-90DS manual heat transfer machine was used to continuously vary temperature from 30°C to 100 °C. Temperature and liquid displacement were video-recorded. The initial state, at 25°C, is shown in Figure 18. The detection range of a temperature tag was 30°C to 100 °C with resolution of 3.1 °C in 10 testing trials.

Table 1. Ranges and Resolution of the Pressure tag, the Bend tag, the Temperature tag and the Gravity tag.

Tag Type	Range	Resolution
Pressure	0.02 – 0.49(N)	34mN
Bend	17 – 31($^{\circ}$)	1.2 $^{\circ}$
Temperature	30 – 100($^{\circ}C$)	3.1 $^{\circ}C$
Gravity	0 – 270($^{\circ}$)	90 $^{\circ}$

5.3.4 Gravitation tests. The range of gravity tag depended on the relative positions of three antenna chips and the total amount of injected liquid in the chamber. In this test, we aligned chips with the chamber centre as Figure 18 and injected liquid to submerge the three chips as the tag posited vertically. In such a design, the liquid submerged only one chip at 90 $^{\circ}$ and 270 $^{\circ}$ rotation and none chip at 180 $^{\circ}$. Our gravity tag range in 270 $^{\circ}$ and resolute at 90 $^{\circ}$.

5.4 User Study: User value of MicroFluID

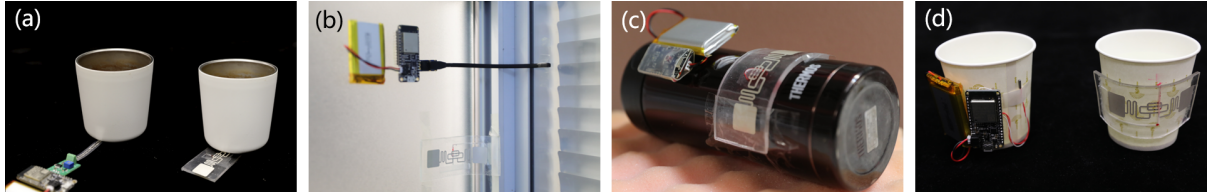


Fig. 19. User study setup of (a) Pressure; (b) Bending; (c) Gravity; and (d) Temperature tags.

To examine the user value of MicroFluID, we conducted a user study with 6 participants (2 males, average age of 30) who had few experiences in prototyping sensing devices. MicroFluID system was compared with other sensing systems, including thin-film force sensors (RFP-611) for pressure, flex sensors (Bend Labs) for bend scenarios, IMU sensors (HII221) for gravitational scenarios, and platinum resistance sensors (PT100) for temperature scenarios, in four scenarios: 1) placing objects on mat coasters, 2) opening the door, 3) knocking over bottles, 4) tasting the temperature of drinking water in a teacup. The adaptive system used ESP32 as a microcontroller, computed data simultaneously on computers via wifi, and was powered by a 3.7V 2000 mAh lithium battery to process signals from the various sensors, as shown in Figure 19. After introduction of setup guidance, users were asked to rate the two detection technologies on a 5-point Likert scale (one score for preferring the comparative method, five for the MicroFluID system) and interviewed at the end.

Results show that users preferred MicroFluID system for activity detection (average score of 4.08). Table 2 shows the average setup period for two detection technologies (4 v.s. 17.5 seconds) and summarizes the pros and cons identified by the users. In general, users preferred MicroFluID, since it was more straightforward, no computation or time cost appeared in learning-based method, easy to deploy, battery-free, and avoided complicated initialization process. However, they wanted MicroFluID to be thinner, making it easier to bend and fold.

6 DISCUSSION

We have shown MicroFluID as a novel RFID sensing artifact to retrieve switchable ID information corresponding to external physical events based on a microfluidic switch circuit. A clear benefit of this approach is that it

Table 2. The benefits of other competing methods.

Methods	Setup time(s)	Pros	Cons
MicroFluID	4	One-off learning Short setup periods No calibration High precision	Low precision Limited detection statuses
Competing methods	17.5		Adaptive setup methods for each technique Waiting for initialisation to complete Needs of battery charging

achieves interaction directly by reading IDs, which helps save a lot of training and calibrating effort that would otherwise be needed in machine learning approaches interpreting primitive phase and signal strength of the tag signals. MicroFluID has potentials in sensing various events as such passive modified RFID tags can be easily attached to different objects. Meanwhile, we are aware of several key challenges and limitations of the work that are worth to be discussed here.

Potential Applications. Based on different external driving forces/stimuli exerting to the liquid inside, MicroFluID possesses various microfluidic switch circuit designs, making it capable of different sensing purposes and compatible with a large variety of scenarios. Here we briefly list some to point out future potential deployment of MicroFluID. For Pressure sensor, it can be applied to a chair back to detect people presence, or to be embedded into shoes to detect footsteps. For Bend sensor, we can apply it to domestic environments such as doors and windows to monitor their closed or opened status. We can even apply it as a wearable device to detect body activities such as wrist movement. User scenarios for Temperature sensor are straightforward, for instance with oven, water bottles to monitor their real-time temperature change. It can also be applied to alert an object breaking thermal threshold. For Gravity sensor, we can use it on steering wheels to detect twisting angles, as well as daily boxes or water bottles that shall be kept in the upright position to monitor if they fall.

Multi-chip RFID Design. The multi-chip RFID antenna design is not a new concept, and it has been used in previous research to work as a thermal alert [?], capture large frequency shift [?], and discrete finger input gestures [?], etc. We extended this by including a microfluidic circuit to support reversible action and more sensing granularity. In the current design, it is straightforward to add more granularity by including more chips placed in parallel. However, it comes at the cost of significantly more tuning effort, which is non-trivial. In our case, we have found a clear effect on the antenna performance of having more than one chip being activated. In addition, in our current design, getting more than one chip connected actually establishes additional parallel circuits, where the antenna's self-inductance, stray capacitance, and resistance loss got changed, causing the impedance mismatch problem. This would further add complexity to tuning the antenna. In this work, we conducted a simulation experiment via HFSS to better understand the EM/RF component of the tag, including the configuration of the proposed multi-chip antenna design, the vector current distribution, the simulated input impedance and the simulated active reflection coefficient, in different states. We also validated the simulation results by analyzing the actual measurements in respect of detectable ranges, which found matched results. However, we understand that actual tests involve more environmental complexity and prototype variances. In our future work, we shall optimize the antenna design, following a strict and iterative process to tune its design parameters to configure the optimal resonant frequency.

Microfluidic Switch Circuit Design and Fabrication. The microfluidic switch circuit used microfluidic mechanism to build switch circuits, which now contains four types of circuits, aiming to detect pressure, bend, temperature

and gravity. As there are still other forms of motion in daily activities (stretch, for example), such design could be expanded according to similar principles to support new modalities. Another challenge is that integrating the switch circuit with the antenna would also affect the design frequency of the antenna, which should be concerned while tuning the multi-chip RFID antenna. Though we had conducted a preliminary fatigue test, sealing problem might appear owing to causes like environment changes or misuses. More preferable fabrication methods should be adopted, for example, changing the material, improving 3D printing precision, to obtain tighter chemical bonds between the two layers.

Conductive Liquid. We have attempted to inject highly conductive liquid inside the microfluidic channel such as liquid metal, which could be identified 10 meters away under domestic environment. However, after being exposed to the air, liquid metal would be oxidised and stick inside the microfluidic channel, in the end scrapping the tag. If considering using it, more process is required. In experiment, we found that water maintains better fluidity, but easy to evaporate. Alcohol and oil could reduce evaporation risk, but their poor electrical properties hampered the overall functionality. Thus, water was chosen in the end. For future work, more types of conductive fluids should be tested to achieve more outstanding performance. In addition, injecting conductive liquid into the microfluidics channel would further change the impedance of the whole antenna, which raises another challenge while tuning the multi-chip RFID antenna.

Assessment. In feasibility assessment section, we mainly focused on the reflected signals of the tag, indicating that our design could support user scenarios in laboratory environment, proving MicroFluID's potential in detecting pressure, bend, gravity and temperature. However, a more systematic experiment with both signal analysis and force-flow displacement quantitative analysis is necessary. This would help us better understand where and how the artifacts shall be applied in practical applications.

During the assessment, we discovered that RFID reader could be adjusted to a relatively high sampling rate in experiments. Thus, if the tag experiences a periodic external force causing changes in identification mode, signals detected by the reader will also be periodic, though the distance between tag and reader might affect reader's sampling rate. In the future, we could deploy these high-frequency characteristics to achieve more uses. It should be mentioned that all of our experiments were accomplished under lab conditions. For more scenarios (office, domestic, etc), further evaluation should be adopted.

In the evaluation of the interaction performance of MicroFluID, we focused on the tag's capabilities in different sensing modals, including their sensing range and resolution. However, it is worth noticing that the tests were based on our current implementations of the prototype, and the values could vary depending on the parametric design of the microfluidic switches, e.g., the channel size, length, inner liquid and air pressure. It is also important to know that MicroFluID has limited sensing granularity, e.g., 5 states for a single setup. The resolution reported can be used as a reference but the designers need to consider the interaction requirements in actual scenarios to determine a best-suited sensing range and resolution.

Size of the Design. Our current prototype is relatively large in size, which cannot be attached to small products such as pencils and earphones. However, the size of the tag is majorly determined by the size and the design of the antenna, as smaller antenna with similar design might restrict energy taking in, hence occluding its functionality. In the future, we will investigate other designs which have smaller sizes. Currently, our prototype has the thickness of 2mm, due to 3D printing prototyping and PDMS casting approach. In the future, by using lithography, thickness of the prototype can reach under 0.2mm.

7 CONCLUSION

This paper presents MicroFluID, a microfluidic switch and a multi-chip structure based RFID tag that reacts to a user's bending or pressing actions, or state changes with orientations or temperatures. MicroFluID takes a

multi-chip antenna design approach. Each combination of activated chips corresponds to a certain input status, and totally takes up to 6 states. This helps reduce the burden of existing deep learning approaches that require significant efforts in data collection and training. The paper makes a thorough description of the structure design and fabrication process, and evaluates the performance of each prototype in lab experiments as well as how users perceive the technique compared with other approaches for similar functions. Results show that MicroFluID is a valid and reliable approach and able to react accurately to applied physical deformations and state changes in the range of around 3 meters.

ACKNOWLEDGMENTS

Our work was supported by Natural Science Foundation of China (No. 61972387) and Key Research Program of Frontier Sciences, CAS (Grant No. QYZDY-SSW-JSC041). We thank all who participated in the user study section and those putting forward valuable suggestions during our design and fabrication process.